Dynamics of reactions at surfaces

Axel Groß

Institut für Theoretische Chemie, Universität Ulm, 89069 Ulm/Germany

I. INTRODUCTION

Chemical reactions correspond to dynamical events involving bond-making and bond-breaking processes [1]. In the previous chapter we have seen how the energetics of catalytic reactions can be determined from first principles using electronic structure theory. Due to the constant improvement in the computer power and the development of efficient algorithms for electronic structure calculations, mainly based on density functional theory (DFT), it has become possible to map out entire potential energy surfaces (PES) of complex catalytic reactions [2, 3]. However, this static information is often not sufficient to really understand how a reaction proceeds. Furthermore, in the experiment the potential energy surface is never directly measured but just reaction rates and probabilities which are a consequence of the interaction potential.

Thus for a true detailed understanding of reaction mechanisms dynamical simulations can be very helpful. Calculating the time evolution of processes also allows a genuine comparison between theory and experiment since experimentally accessible quantities such as reaction or adsorption probabilities can be directly derived from the simulations. Thereby dynamical simulations also provide a reliable check of the accuracy of the calculated PES on which the dynamical simulations are based.

In Fig. 1, a schematic two-dimensional PES is shown as a function of the distance of the reactants from a catalyst surface and of some molecular coordinate. It provides an illustration how a catalyst works. A reaction might be hindered by a relatively large barrier in the gas phase or in solution. However, for the adsorbed reactants, the barrier can be much lower. Thus the catalyst provides a detour in the multi-dimensional configuration space with a barrier that can be much more easily traversed.

It should be noted that the catalyst not only provides reaction routes with smaller barriers, but the catalyst also acts as a thermal bath that can provide and dissipate energy. Therefore many details of heterogeneous catalytic reactions can be understood based on concepts derived from equilibrium thermodynamics. For example, rate constants can be estimated based on transition state theory [4] where the assumption of strong friction is crucial [5]. This also means that the activity and selectivity of a heterogeneous catalytic reactions depend much more strongly on activation barrier heights, which enter the reaction rate constants exponentially, than on dynamical effects. This means that the length and the curvature of the detour in the multi-dimensional configuration space illustrated in Fig. 1 hardly matters, it is just the reduction in the activation barrier height on the
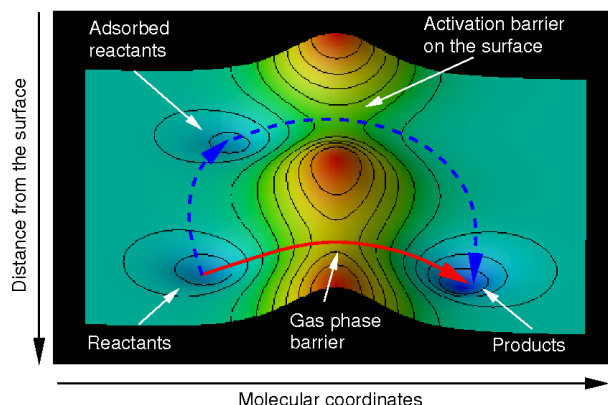

FIG. 1: Schematic illustration of the role of a catalyst employing a two-dimensional representation of the potential energy surface. A catalyst provides a detour in the multi-dimensional PES (dashed line) with a lower activation barrier for the adsorbed species than in the gas phase (or in solution).

catalyst surface that accelerates the reaction.

Furthermore, activated processes usually correspond to rare events so that their dynamical description would involve the simulation of many unsuccessful events which is rather time-consuming and thus not reasonable. For such processes, coarse-grained dynamical methods such as kinetic Monte Carlo simulations [6, 7] which are also presented in this volume are much more appropriate.

Still, there are certain processes in catalytic reactions whose probability can not be determined using transition state theory. The most prominent example is atomic and non-dissociative molecular adsorption: here the adsorption probability strongly depends on the dissipation of the kinetic energy of the impinging atom or molecule which can only be determined in dynamical simulations [8].

In this chapter, I will show what kind of information about heterogeneous catalytic reactions can be gained by studying the dynamics of reactions at surfaces. I will first discuss the theoretical and computational methods required to perform dynamical simulations. Most of the dynamical simulations are based on the Born-Oppenheimer or *adiabatic* approximation taking advantage of the difference in the mass between nuclei and electrons. Furthermore, in principle the atomic motion should be described by a quantum mechanical treatment, but it turns out that classical mechanics is often sufficient.

In order to perform dynamical simulations, the potential energy surface and its gradients are needed at arbitrary points of the configuration space. However, electronic structure calculations only yield energies at dis-

crete points of the configuration space. Hence one uses either reliable interpolation methods for a continuous representation of the PES on which the dynamical simulations are performed, or one employs methods where the gradients are calculated "on the fly". Such *ab initio* molecular dynamics (AIMD) simulations are rather time-consuming but I will show that it has become possible to determine a sufficient number of trajectories in order to obtain statistically significant results [9].

Most of the examples I will show are related to adsorption processes and simple reactions on surfaces. As mentioned above, such processes can usually be described employing the Born-Oppenheimer approximation. However, there are important examples of catalytically relevant reactions where this approximation breaks down. The dynamical treatment of electronically non-adiabatic reactions at surfaces is rather complex, but I will show that such reactions can also be treated from first principles nowadays.

II. THEORETICAL AND COMPUTATIONAL FOUNDATIONS OF DYNAMICAL SIMULATIONS

In the realm of chemistry and solid-state physics, there is only one basic interaction which is relevant, namely the electrostatic interaction between the charged nuclei and electrons. Thus together with the kinetic energy of the nuclei and the electrons only the nucleus–nucleus, nucleus-electron and electron-electron electrostatic interaction energy enter the Hamiltonian describing catalytic systems:

$$H = T_{\mathrm{nucl}} + T_{\mathrm{el}} + V_{\mathrm{nucl-nucl}} + V_{\mathrm{nucl-el}} + V_{\mathrm{el-el}} \tag{1}$$

Relativistic effects are usually negligible except for the heaviest elements where the high charge of the nucleus can accelerate the electrons to velocities close to the speed of light. Thus typically catalytical systems are described by the nonrelativistic Schrödinger equation

$$H \, \Phi(\mathbf{R}, \mathbf{r}) = E \, \Phi(\mathbf{R}, \mathbf{r}) \tag{2}$$

where $\mathbf{R}$ and $\mathbf{r}$ denote *all* nuclear and electronic coordinates, respectively. In principle, one is ready here because complete knowledge about the system can be gained by solving the Schrödinger equation and determining the eigenfunctions of the many-body Hamiltonian taking into consideration the proper quantum statistics of the particles. Unfortunately, the solution of the many-body Schrödinger equation in closed form is not possible. Thus a hierarchy of approximations is needed in order to make the solution feasible.

The first approximation that is typically used is the Born–Oppenheimer or adiabatic approximation [10]. Its central idea is the separation in the time scale of processes involving electrons and atoms because of their large mass

mismatch. Typically, at the same kinetic energy electrons are 10^2 to 10^3 times faster than the nuclei. Hence one assumes that the electrons follow the motion of the nuclei instantaneously.

In practice, one splits up the full Hamiltonian and defines the electronic Hamiltonian H_{el} for fixed nuclear coordinates $\mathbf{R}$ as follows

$$H_{\mathrm{el}}(\{\mathbf{R}\}) = T_{\mathrm{el}} + V_{\mathrm{nucl-nucl}} + V_{\mathrm{nucl-el}} + V_{\mathrm{el-el}}. \tag{3}$$

In Eq. (3), the nuclear coordinates $\{\mathbf{R}\}$ do not act as variables but as parameters defining the electronic Hamiltonian. The Schrödinger equation for the electrons for a given fixed configuration of the nuclei is then

$$H_{\mathrm{el}}(\{\mathbf{R}\})\Psi(\mathbf{r}; \{\mathbf{R}\}) = E_{\mathrm{el}}(\{\mathbf{R}\})\Psi(\mathbf{r}; \{\mathbf{R}\}). \tag{4}$$

This is the basic equation of quantum chemistry that is solved by electronic structure codes, either using wave function based methods or density functional theory, as described in the previous chapter. In the Born–Oppenheimer approximation, the eigenenergies $E_{\mathrm{el}}(\{\mathbf{R}\})$ of the electronic Schrödinger equation as a function of the nuclear coordinates $\{\mathbf{R}\}$ define the potential for the nuclear motion. $E_{\mathrm{el}}(\{\mathbf{R}\})$ is therefore called the Born–Oppenheimer energy surface. Minima of the Born-Oppenheimer surface correspond to stable and metastable configurations of the system, for example energy minimum structures of molecules or adsorption sites on a surface, whereas saddle points are related to activation barriers for chemical reactions or diffusive motion.

The validity of the Born-Oppenheimer approximation is hard to prove. Still it has been very successful in the theoretical description of chemical reactions. Qualitatively, two regimes can be identified in which the Born-Oppenheimer approximation should be justified. If there is a large energy gap between the highest occupied molecular orbital (HOMO) and the lowest unoccupied molecular orbital (LUMO) in the case of molecules or between the valence and the conduction band in the case of solids, then electronic transitions will be rather improbable and the system is likely to stay in the electronic ground state. If, on the other hand, there is no band gap, like in the case of metals, but there are many coupled electronic states allowing electronic transitions with arbitrarily small excitation energies, then the strong coupling of the electronic states in the broad conduction band will lead to short lifetimes of excited states and thus to a fast quenching of these states. The Born-Oppenheimer approximation breaks down if either electronic states are directly excited like in photochemistry or if there are few weakly coupled electronic states so that there is a small probability for the system to relax to the electronic ground state. Such systems require a special treatment, as will be shown in section VIII.

Within the Born-Oppenheimer approximation, the quantum dynamics can be determined by solving the atomic Schrödinger equation

$$\{T_{\mathrm{nucl}} + E_{\mathrm{el}}(\mathbf{R})\} \Lambda(\mathbf{R}) = E_{\mathrm{nucl}}\Lambda(\mathbf{R}) \,, \tag{5}$$

where $E_{\text{el}}(\mathbf{R})$ acts as the potential. However, often quantum effects in the atomic motion can be neglected and the classical equation of motion are solved for the atomic motion:

$$M_I \frac{\partial^2}{\partial t^2} \mathbf{R}_I = -\frac{\partial}{\partial \mathbf{R}_I} E_{\text{el}}(\mathbf{R}) \ . \qquad (6)$$

This is the basis for molecular dynamics (MD) simulations. The interaction potential $E_{\text{el}}(\mathbf{R})$ does not necessarily have to be derived from first principles. In particular for biological systems, there are parameterized interaction potentials available, so-called *force fields* which are often derived from a combination of experimental and theoretical data. However, such *classical* potentials are usually not well-suited to describe bond-making and bond-breaking processes, as they occur in heterogeneous catalytic reactions. Hence I will here only discuss dynamical simulations that are based on first-principles calculations.

III. INTERPOLATION OF POTENTIAL ENERGY SURFACES

In order to perform *quantum* dynamical simulations, a continuous presentation of the potential energy surface is needed since the wave functions are delocalized and always probe a certain extended area of the PES at any time. On the other hand, classical molecular dynamics simulations on a suitable analytical representation of a potential energy surface can be extremely fast. First-principles total energy calculations, however, just provide total energies for discrete configurations of the nuclei. Hence it is desirable to adjust the first-principles energies to an analytical or numerical continuous representation of the PES. This is a not an easy task. The representation should be flexible enough to accurately reproduce the ab initio input data, yet it should have a limited number of parameters so that it is still controllable. Furthermore, a good parameterization should not only accurately interpolate between the actually calculated points, but it should also give a reliable extrapolation to regions of the PES that have actually not been determined by the first-principles calculations.

A straightforward approach is to assume a certain analytical form of the interaction potential $V(\mathbf{R})$ depending on a certain number of parameters [12, 13] and then adjust these parameters in such a way that the root mean square error (RMSE)

$$\Delta E_{\text{RMSE}} = \sqrt{\frac{1}{N} \sum_i^N (V(\mathbf{R}_i) - E_{\text{el}}(\mathbf{R}_i)^2} \qquad (7)$$

is minimal, where the $\mathbf{R}_i$ are the N configurations for which the energy has been evaluated by first-principles calculations. Such an approach has for example been used to interpolate the PES of the interaction of H_2 with
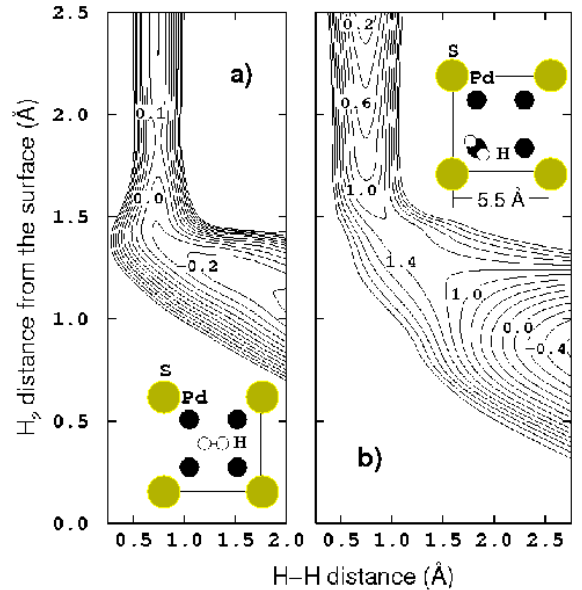

FIG. 2: Two-dimensional cuts through the potential energy surface of $H_2/S(2\times2)/Pd(100)$ derived from DFT calculations as a function of the H-H distance and the H_2 distance from the surface. The insets illustrate the molecular orientation and lateral center of mass position. The contour spacing in a) is $0.1\,\text{eV}$ while it is $0.2\,\text{eV}$ in b). (After [11])

a Pd(100) surface covered by a quarter monolayer of sulfur within a $S(2 \times 2)/Pd(100)$ geometry [11, 14]. Two so-called elbow plots of this PES, i.e., two-dimensional cuts through the multi-dimensional PES as a function of the interatomic H-H distance and the H_2 center of mass distance from the surface for different lateral positions and orientations of the H_2 molecule, are shown in Fig. 2. Typically, these interaction potentials are strongly corrugated and anisotropic, i.e., they sensitively depend on the lateral position and orientation of the molecule, even for smooth metal surfaces [15].

If more than just the molecular degrees of freedom should be considered in a parameterization of an ab initio PES, analytical forms become very complicated and cumbersome. Furthermore, sometimes analytical expression introduce some artificial symmetries into the description of the PES which can have quite a significant influence on dynamical results [9]. There are some numerical schemes which avoid the restrictions of analytical expansions. Neural networks can fit, in principle, any real-valued, continuous function to any desired accuracy. They have already been successfully applied to interpolate ab initio potential energies describing chemical reactions [16–20]. Another approach is to use a modified Taylor expansion of the PES around the points calculated from first-principles [21]. One disadvantage of these numerical schemes is that there is no physical insight used as an input in this parameterization. Hence the parameters of the expansions do not reflect any phys-

ical or chemical property which usually leads to a large number of unknowns in the parameterization.

There are some interpolation methods that are not purely numerical. For example, the corrugation-reducing procedures [22–25] takes advantage of the observation that most of the corrugation in molecule-surface potential energy surfaces can already be derived from the atom-surface interaction. In this method, the interaction of both the atomic and the molecular species with the surface is determined by first-principles calculations. Then a three-dimensional reference function is constructed from the atomic data which is subtracted from the molecular potential energy surface. The remaining function is much smoother than the original potential energy surface and therefore much easier to fit, and furthermore, the interpolated PES also reflects the correct symmetry of the system. This method has been used successfully for quite a number of interaction potentials [22–24, 26, 27]. Still, this method can not easily been extended to include surface degrees of freedom.

As an intermediate method between purely numerical schemes and full first-principles calculations the representation of the ab initio interaction potential by a tight-binding formalism was suggested [28]. Tight-binding methods are more time-consuming than an analytical representation or a neural network since they require the diagonalization of matrices. However, due to the fact that the quantum mechanical nature of bonding is taken into account [29], a smaller number of ab initio input points is needed in order to perform a good interpolation [30]. Furthermore, tight-binding schemes can even used for the extrapolation of first-principles results since the parameters of the tight-binding scheme, the Slater-Koster integrals [31], have a well-defined physical meaning. This makes for example the inclusion of lattice vibrations possible [32, 33], as will be shown in this chapter.

Finally, it should be emphasized that it is not trivial to judge the quality of the fit to a first-principles PES. Using just the integrated value of the root mean square error Eq. (7) is often not sufficient since some points of the potential energy surface, for example activation barriers, are more important than others. This can be taken into account by introducing weighting factors in the formulation of ΔE_{RMSE}.

IV. QUANTUM DYNAMICS OF REACTIONS AT SURFACES

In order to treat the quantum dynamics of reactions at surfaces, either the time-dependent Schrödinger equation

$$i\hbar \frac{\partial}{\partial t} \Psi(\vec{R}, t) = H \Psi(\vec{R}, t) \qquad (8)$$

or the time-independent Schrödinger equation

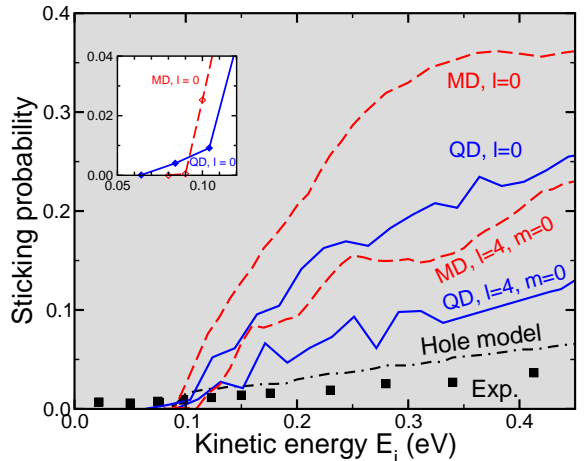$$H \Psi(\vec{R}) = E \Psi(\vec{R}, t) \qquad (9)$$

FIG. 3: Quantum dynamical (QD) and classical (MD) dissociative adsorption probability of hydrogen on sulfur-covered Pd(100) as a function of the initial kinetic energy for initially non-rotating (l=0) and rotating H_2 molecules (l=4). (after [44]). In addition, experimental results [46] and the integrated barrier distribution (denoted by "hole model" [47]) are included.

may be solved. Both approaches are equivalent and should lead to the same results. The time-dependent Schrödinger equation is typically solved on a numerical grid using the wave-packet formalism [34–37]. In the time-independent formulation, the wave-function is usually expanded in some suitable set of eigenfunctions leading to so-called *coupled-channel equations* [38, 39]. High-dimensional quantum dynamical simulations are computationally rather expensive. Still it is nowadays possible to describe the interaction dynamics of H_2 with metal surfaces including all six degrees of freedom of the H_2 molecule dynamically [13, 40–43], even at precovered [11, 44] and stepped [45] surfaces. However, the computational effort grows exponentially with the number of degrees of freedom considered, and hence it is almost impossible to include substrate degrees of freedom realistically in these quantum simulations.

One of these high-dimensional quantum studies was devoted to the H_2 dissociation on sulfur-precovered surfaces [11, 44]. This study is of relevance for heterogeneous catalysis since sulfur is known to act as a catalyst poison, i.e., its presence reduces the catalytic activity of a substrate. DFT calculations have shown that the poisoning of sulfur is due to a combination of direct and indirect effects [14, 48]. Since sulfur is strongly bound to Pd(100) it first of all blocks sites at which no further reaction can take place. But secondly, it also modifies the electronic structure of the Pd substrate. The interaction of sulfur with Pd leads to a down-shift of the Pd *d*-states. As a consequence, in the vicinity of sulfur atoms on Pd the H_2 dissociation is no longer non-activated, as on the clean Pd surface [49], but a dissociation barrier is build up. Such a barrier of height 0.1 eV is shown in Fig. 2a above the hollow position. When the H_2 molecule is moved
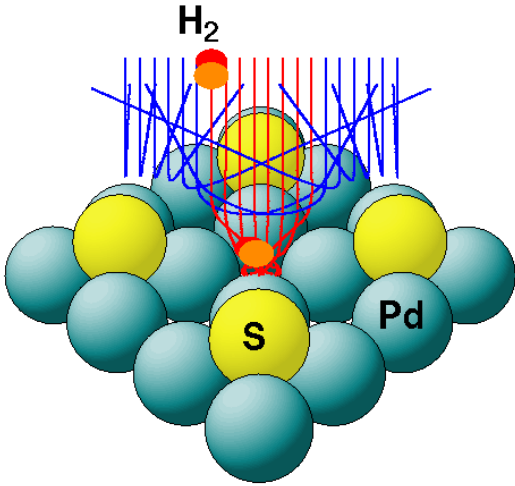
FIG. 4: Illustration of the redirection of H_2 molecules upon approaching the highly corrugated $S(2 \times 2)/Pd(100)$ surface. The lines correspond to the calculated classical trajectories tracing the H_2 center of mass. Both scattering and adsorption events are depicted. Upon adsorption, not only the H_2 center of mass is redirected, but also the molecular orientation is changed.

towards the sulfur atom, then the direct repulsion between H_2 and sulfur leads to a dramatic increase in the dissociation barrier height. While this barrier above the top site of clean Pd(100) has an value of 0.15 eV [49], it rises to more than 1.2 eV above Pd atoms close to the adsorbed sulfur atoms (see Fig. 2b). This results in a strongly corrugated PES.

In order to study the dynamical consequences of the sulfur-poisoning on the hydrogen adsorption dynamics, a six-dimensional quantum dynamical study was performed [11, 44]. Figure 3 shows calculated sticking probabilities as a function of the initial kinetic energies for initially non-rotating and rotating molecules. In addition, results according to the so-called *hole model* [47] are plotted. This is the integrated barrier distribution $P_{\rm b}(E)$ which is the fraction of the configuration space for which the barrier towards dissociation is less than E. and it would correspond to the sticking probability if the impinging H_2 molecules are not redirected and deflected upon the approach towards the surface.

The fact that the calculated sticking probabilities are all significantly larger than the results according to the hole model indicates that there are considerable dynamical effects during the dissociative adsorption in this system. As already mentioned, the PES of H_2 interacting with $S(2 \times 2)/Pd(100)$ is strongly corrugated. In addition, it is also highly anisotropic. As a consequence, molecules directed towards high barriers are very efficiently steered to configurations and sites with lower barriers [40]. This process is illustrated in Fig. 4 where the calculated center-of-mass traces of H_2 molecules scattering and adsorbing on $S(2 \times 2)/Pd(100)$ are plotted.

The high anisotropy of the PES is also reflected in the strong dependence of the sticking probability on the initial rotational state of the molecules. When the molecules are initially in a rotational state corresponding to the rotational quantum number $l = 4, m = 0$, the sticking probability is significantly reduced compared to the sticking probability for initially non-rotating molecules ($l = 0$). This rotational hindering is caused by the fact that rapidly rotating molecules rotate out of molecular orientations favorable for dissociation during the interaction with the surface. Invoking the principle of detailed balance or microscopic reversibility between adsorption and desorption, the rotational hindering in adsorption is reflected by so-called rotational cooling in desorption, i.e., the mean rotational energy of desorbing molecules is less than expected for molecules in thermal equilibrium at the surface temperature. This rotational cooling was indeed observed in experiments and reproduced in quantum dynamical calculations, not only at sulfur-covered Pd(100) [50], but also at clean Pd(100) [51].

There are further dynamical aspects of the interaction dynamics of H_2 at $S(2 \times 2)/Pd(100)$ which are quite general and have been also found in other systems [52]. Not only the rotational motion, but also the orientation of the rotating molecules matters. Molecules rotating in the so-called helicopter mode with their molecular axis parallel to the surface have a higher dissociation probability than molecules rotating in the cartwheel mode for which the *rotational* axis is parallel to the surface [44]. This is caused by the fact that molecules in the cartwheel mode have a high probability of hitting the surface in an upright configuration which is rather unfavorable for dissociative adsorption [14, 48]. The stereodynamical consequences can again best been observed in desorption where this anisotropy leads to rotationally aligned molecules [44, 53]. In addition, initial vibrational motion enhances the sticking probability and leads to vibrational heating in desorption [50]. However, the vibrational effects are much less pronounced than in so-called late barrier systems, such as H_2/Cu [37, 41, 52, 54, 55] where in contrast to the $H_2/S(2 \times 2)/Pd(100)$ PES shown in Fig. 2 the barrier for dissociation is located after the curved region of the reaction path. Such a topology of the PES leads to a very efficient coupling between translational and vibrational motion.

Although qualitatively all experimentally observed dynamical aspects of the reaction dynamics of H_2 at $S(2 \times 2)/Pd(100)$ are reproduced by the first-principles based simulations, there are still significant quantitative differences, in particular as far as the sticking probability shown in Fig. 3 is concerned. The experimental results are much smaller than the calculated ones. First of all one has to note that the dynamical simulations are only of approximate nature. The calculated PES might not be fully correct due to problems associated with current DFT functionals [56]. Furthermore, the neglect of electronic excitations and the substrate motion in the dynamical simulations could have an influence on the ac-

curacy of the results. However, it should also be noted that experimentally the preparation of an ordered (2×2) sulfur overlayer on Pd(100) is not trivial [46, 50]. Sulfur tends to form a $c(2 \times 2)$ overstructure on Pd(100) [50] corresponding to a higher coverage which would explain the low sticking probability observed in the experiment [46].

Finally, the difference between quantum dynamical results and classical results, which are also included in Fig. 3, shall be discussed. There are basically two quantum effects which are absent in classical dynamics: tunneling and zero-point and quantization effects due to the localization of the wave function perpendicular to the reaction path, in particular in the so-called frustrated modes which are free in the gas phase. In fact, these two quantum effects have opposite consequences compared to classical results. Tunneling leads to additional particles that cross the barrier whereas zero-point effects typically lead to an effective increase in the barrier heights which reduces the sticking probability. However, one has to note that upon dissociative adsorption the intramolecular vibration becomes softer leading to a decrease of the zero-point energy in this mode which can compensate the increase in the zero-point energies is all other modes [57]. The fact that the quantum sticking probabilities are smaller than the classical sticking probabilities (see Fig. 3) indicates that zero-point effects due to the frustrated modes are more dominant than tunneling in the quantum dynamics of the $H_2/S(2 \times 2)/Pd(100)$. This is also true for H_2 dissociation on other metal surface [13].

Another quantum effect is the relatively strong structure of the quantum sticking probability as a function of the kinetic energy due to resonance effects and the opening up of new scattering channels with rising kinetic energies [13]. Such quantum oscillations have not been observed yet despite significant experimental efforts [58]; they are quickly washed out by imperfections of the substrate and thermal motion of the surface atoms [59]. Furthermore, it should be noted that in spite of the quantitative differences between quantum and classical results in Fig. 3 qualitatively they show the same behavior as a function of the initial kinetic energy and the initial rotational states. This means that classical molecular dynamics simulations can be used to get qualitative trends in the reaction dynamics at surfaces even for the lightest element hydrogen; for heavier atoms the quantum effects are actually less pronounced so that the results of classical molecular dynamics simulations become rather reliable.

V. NONDISSOCIATIVE MOLECULAR ADSORPTION DYNAMICS

For the simulation of the dissociative adsorption dynamics of H_2 on metal surfaces, the recoil of the substrate atoms usually does not play a crucial role because of the large mass mismatch between metal and hydrogen
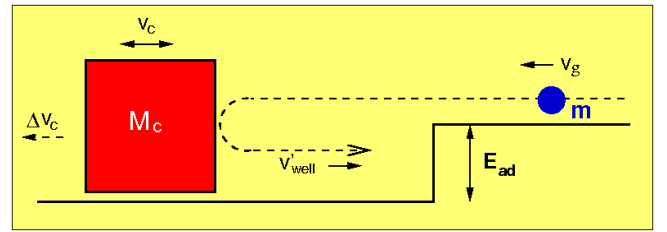

FIG. 5: Schematic illustration of the hard cube model [60, 61]. An atom or molecule with mass m is impinging in an attractive potential with well depth E_{ad} on a surface modeled by a cube of effective mass M_c. The surface cube is moving with a velocity v_c given by a Maxwellian distribution.

atoms. After dissociation, the single hydrogen atoms will eventually accommodate at the surface due to the dissipation of their kinetic energy to the substrate, but the energy transfer to the substrate hardly influences the dissociation probability.

This situation is entirely different for atomic and nondissociative molecular adsorption. In order to stick to the surface, the impinging atoms and molecules have to transfer their initial kinetic energy to the substrate, i.e., the sticking probability as a function of the initial energy E can be expressed as

$$S(E) = \int_E^\infty P_E(\epsilon) \, d\epsilon \, , \qquad (10)$$

where $P_E(\epsilon)$ is the probability that an incoming particle with kinetic energy E will transfer the energy ϵ to the surface. This energy will mainly be taken up by substrate vibrations, but also the excitation of electron-hole pairs at the surface can contribute to the dissipation, as will be discussed below.

Typically the sticking probability in atomic or nondissociative molecular adsorption decreases as a function of kinetic energy because the energy transfer to the substrate becomes less efficient at higher kinetic energies [39]. The qualitative features of nondissociative adsorption can be discussed within the so-called *hard cube model* (HCM) [60, 61] in which the impact of the atom on the surface is treated as a binary elastic collision between a gas phase atom (mass m) and a substrate atom (mass M_c) which is moving freely with a velocity distribution $P_c(v_c)$. Close to the surface, the particle becomes accelerated because of the adsorption well of depth E_{ad}. This model that is illustrated in Fig. 5 can be solved analytically. Thus it can be shown that the sticking probability becomes higher for larger well depth E_{ad} and greater mass ratio m/M_c because then the impact on the surface "cube" becomes stronger and consequently the energy transfer to the substrate is enlarged.

The HCM model has been used to model the energy transfer to the surface in atomic or molecular adsorption [60, 61], for example also for the sticking of O_2 on Pt(111) [62]. However, it assumes that the molecule is a point-like object impinging on a flat surface. This as-
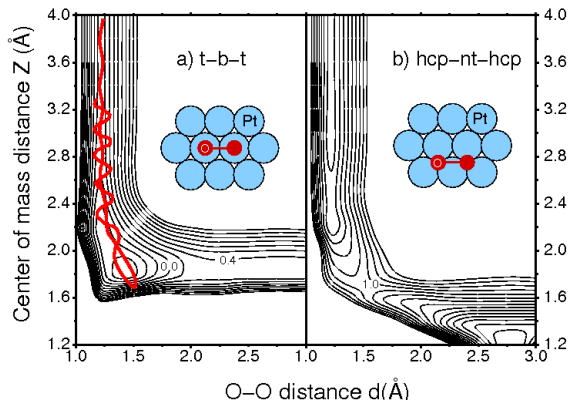
FIG. 6: Two-dimensional cuts through the potential energy surface of O_2/Pt(111) determined by a *ab initio* derived tight-binding Hamiltonian as a function of the O-O distance and the O_2 distance from the surface [32]. The insets in a) and b) illustrate the molecular orientation and lateral center of mass position corresponding to a top-bridge-top (t-b-t) and a hcp hollow-near top- hcp hollow (hcp-nt-hcp), respectively. The contour spacing is 0.2 eV per O_2 molecule. In (a) a trajectory of an O_2 molecule with an initial kinetic energy of 0.6 eV scattered at Pt(111) is also plotted.

sumption is rather crude and can lead to an erroneous interpretation of measured sticking probabilities, as has been shown especially for the O_2/Pt(111) system [32, 33]. This system is of particular importance for the understanding of the elementary processes occuring in the car exhaust catalyst. In spite of its seemingly simplicity this system is rather complex since oxygen can exist in different states on Pt(111). A weakly bound physisorbed species exists at surface temperatures up to 30 K [63, 64]. Chemisorbed peroxo-like (O_2^{-2}) and superoxo-like (O_2^{-}) molecular species are found at surface temperatures below about 100 K [65, 66]. For higher surface temperatures, oxygen adsorbs dissociatively [67].

The chemisorbed O_2 species on Pt(111) have also been identified in DFT total-energy calculations [68, 69]. Two elbow plots of the calculated O_2/Pt(111) PES are shown in Fig. 6. The superoxo molecular precursor state corresponds to the minimum in Fig. 6a above the bridge site with a binding energy of 0.72 eV [68, 69]. The other chemisorption state, the peroxo state which is energetically almost degenerate with the superoxo state, is located above the threefold hollow sites with its axis slightly tilted from the parallel orientation (not shown in Fig. 6). Both chemisorption states can be accessed from the gas-phase without encountering any barrier, i.e., the adsorption in non-activated.

Figure 6b demonstrates the strong corrugation of the O_2/Pt(111) PES. Although the molecule is only shifted by about 1 Å from the bridge position of Fig. 6a to a near-top position, there is no longer any chemisorption well present but rather a large barrier of about 1 eV towards dissociative adsorption. This barrier becomes even larger

for the molecule directly at the on-top site. Furthermore, the PES is also strongly anisotropic: for molecules in an upright orientation, the PES is repulsive. In fact, the majority of adsorption pathways are hindered by barriers; direct non-activated access to the adsorption states is possible for only a small fraction of initial conditions.

Interestingly, molecular beam experiments showed the surprising result that oxygen molecules do not dissociate on cold Pt surfaces below 100 K [62, 70, 71], even at kinetic energies above 1 eV. As Fig. 6a indicates, this energy is much greater than the dissociation barrier which is of the order of 0.2 eV with respect to the gas-phase energy of O_2. Apparently, in the system O_2/Pt(111) the kinetic energy of the impinging molecules is not operative in surmounting the dissociation barrier.

To simulate the adsorption dynamics of O_2/Pt(111) represents in fact a significant theoretical and computational challenge. On the one hand, a realistic PES is needed that reliably describes both the molecular as well as the dissociative adsorption channels. On the other hand, molecular trapping processes can only be reproduced if the energy dissipation to the platinum substrate is properly taken into account. Using empirical classical potentials, almost arbitrarily many trajectories can be computed, however, there are no reliable interaction potentials available treating reactions on the surface and the surface recoil upon impact on an equal footing.

Ab initio molecular dynamics (AIMD) simulations represent a method that is well-suited for this task. For H_2, AIMD simulations of the adsorption dynamics on precovered surfaces were indeed already successfully performed (see the next two sections). However, periodic DFT calculations involving oxygen are computationally much more expensive: on the one hand, the strong localization of the oxygen wave functions close to the nucleus requires a larger plane wave basis, on the other hand, oxygen has to be described in a spin-polarized manner because of its atomic and molecular triplet states. As a compromise, the results of static DFT calculations [68, 69] were used in order to adjust a tight-binding (TB) Hamiltonian [28, 30, 32, 33]. This approach combines a quantum mechanical description of the molecule-surface interaction with the numerical efficiency of tight-binding calculations which are about three orders of magnitude faster than DFT calculations. The elbow plots shown in Fig. 6 were in fact produced using an TB Hamiltonian with its parameter adjusted to reproduce ab initio calculations.

Figure 7 shows sticking probabilities derived from tight-binding molecular dynamics (TBMD) simulations. The results were obtained by averaging over a sufficient number of trajectories with random initial lateral positions and orientations of the O_2 molecules that were started 4 Å above the surface. The classical equations of motion were integrated using the Verlet algorithm [73] with a time step of 1 fs within the microcanonical ensemble. The statistical error ΔS of the calculated sticking probability S can be estimated by

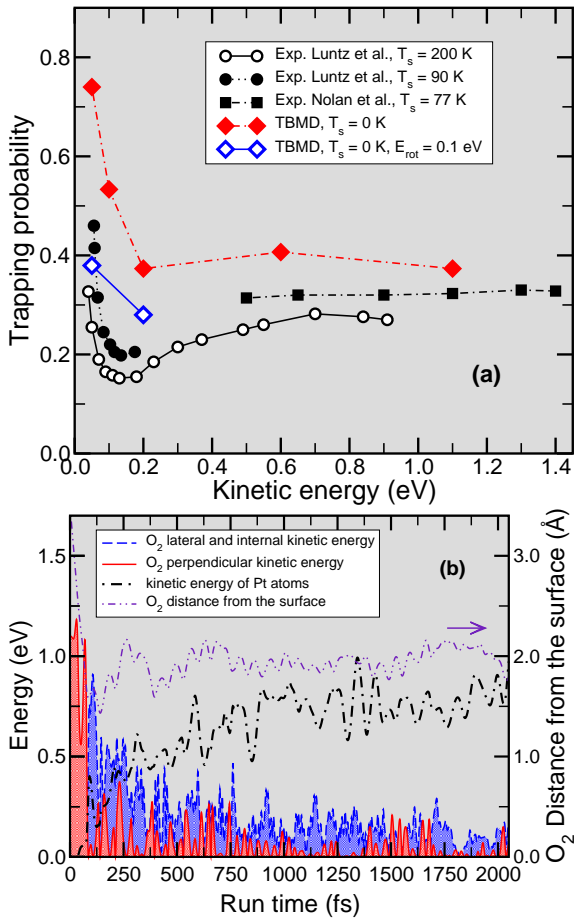$$\Delta S = \sqrt{S(1-S)}/\sqrt{N} , \qquad (11)$$

FIG. 7: Molecular trapping of O_2 on Pt(111). a) trapping probability of O_2/Pt(111) as a function of the kinetic energy for normal incidence. Results of molecular beam experiments for surface temperatures of 90 K and 200 K (Luntz *et al.* [72]) and 77 K (Nolan *et al.* [71]) are compared to tight-binding molecular dynamics simulations for the surface initially at rest ($T_s = 0$ K) for initially rotating and non-rotating molecules. b) Calculated energy redistribution and O_2 center of mass distance from the surface for a O_2 molecule impinging on Pt(111) with an initial kinetic energy of 1.1 eV. Left panel: distance from the surface and energy redistribution as a function of time. The lateral and internal kinetic energy and the perpendicular kinetic energy curves are indicated by the blue and red-shaded areas, respectively.

where N is the number of calculated trajectories. Already for a relatively small number of trajectories such as $N = 200$ the statistical uncertainty of the calculated sticking probability is below 3.5 % which is usually sufficient if the sticking probabilities lie in the range between 0.1 and 1.

Calculated and measured [71, 72] sticking probabilities of O_2/Pt(111) as a function of the kinetic energy are compared in Fig. 7a. There is a semi-quantitative agreement between theory and experiment which is quite satisfactory regarding the numerous approximations entering the calculations. The TBMD simulations also repro-duced the surprising experimental finding that O_2 does not directly dissociate upon adsorption, even at kinetic energies of 1.1 eV.

This peculiar behavior can in fact be understood by inspecting the topology of the elbow plots of O_2/Pt(111). At the energetically most favorable adsorption paths, O_2 is first attracted to the surface towards the molecular chemisorption states. Because it is a nondissociative molecular state, the O-O bond length hardly changes when the molecule enters the chemisorption well. On the other hand, during the dissociation the oxygen atoms remain at roughly the same distance from the surface. As as consequence, there is no smoothly curved energy minimum reaction path towards dissociative adsorption, as for H_2 dissociation plotted in Fig. 2, but rather a sharply bend path, as shown in Fig. 6a. This is also illustrated by a typical trajectory of an O_2 molecule directly aimed at the molecular precursor state that is included in the figure. Its initial kinetic energy of 0.6 eV is much higher than the dissociation barrier so that the molecule could in principle adsorb dissociatively. However, it rather becomes accelerated by the attractive potential, hits the repulsive wall of the potential and is scattered back into the gas phase. It does not enter the dissociation channel since this would correspond to a sharp turn on the potential energy surface.

This does not mean that direct dissociation of O_2/Pt(111) is impossible, but it is very unlikely. Hence, dissociation of O_2 on Pt(111) is usually a two-step process. First the molecule becomes trapped and accommodated in the molecular chemisorption state, and only subsequently it dissociates at sufficiently high surface temperatures due to thermal fluctuations which will make the O_2 molecules enter the dissociation channel.

Furthermore, STM experiments showed that after dissociation upon heating the Pt substrate, the two oxygen atoms are found on the average two Pt lattice units apart from each other [67]. Kinetic Monte Carlo simulations [74] showed that this spatial distribution cannot result from two atomic jumps, but rather from a hot atom movement after dissociation, as will be discussed in detail in section VII.

We will now focus on the sticking probability as a function of the kinetic energy. At low kinetic energies, it first strongly decreases and then it levels off after passing a minimum. This strong initial decrease of the sticking probability was initially interpreted as being caused by the trapping into a shallow physisorption state with a well depth of about 0.12 eV [62, 71]. However, such a shallow physisorption well is not present in the TB-PES, but still this strong decrease is reproduced in the TBMD simulations.

An analysis of the trajectories showed that also at low kinetic energies the molecules enter the chemisorption wells. However, the sticking probability at these low kinetic energies is not determined by the energy transfer to the substrate *per se* but rather by the probability to access the entrance channels towards the chemisorption
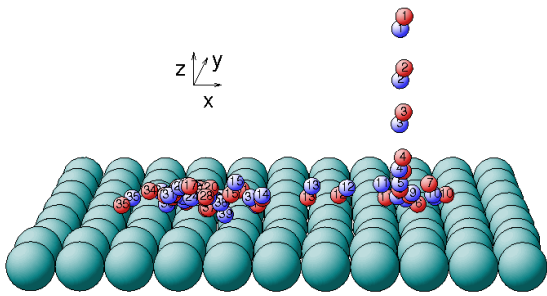
FIG. 8: Illustration of the conversion of the molecular kinetic energy perpendicular to the surface into internal degrees of freedom (rotations, vibrations) and lateral movement across the surface leading to a dynamical precursor state. The snapshots along the trajectory are number consecutively.

states. All molecules that find their way to the molecular chemisorption state at low kinetic energies do in fact remain trapped. At low kinetic energies, a high fraction of the impinging O_2 molecules is indeed steered towards the attractive paths towards the chemisorption states (such a steering is illustrated in Fig. 4). However, this steering effect becomes strongly suppressed at higher kinetic energies [40, 75], and this is the reason for the initial decrease in the sticking probability. This steering effect becomes in fact also suppressed by additional rotational motion. This is reflected in Fig. 7a by the strong reduction in the calculated TBMD sticking probability for O_2 molecules that have initially a rotationally energy of $E_{rot} = 0.1\,eV$.

The leveling off of the sticking probability at higher kinetic energies is also a surprising result. According to the hard-cube model, no O_2 molecules with a kinetic energy of $1.0\,eV$ would stick at a surface with a chemisorption well depth of $0.7\,eV$. However, the hard-cube model assumes the impinging of a point-like particle on a flat surface; it does not take into account the corrugation and anisotropy of the PES.

In Fig. 7b, the energy redistribution along the trajectory of an O_2 molecules impinging on Pt(111) with an initial kinetic energy of $1.1\,eV$ is shown; in addition, the O_2 center of mass distance from the surface is plotted. When the molecules hits the surface for the first time after about $70\,fs$, less than $0.4\,eV$ is transferred to the substrate vibrations. This transfer would not be sufficient for the molecule in order to remain at the surface. Still, almost $1\,eV$ is transferred to lateral and internal (rotations, vibrations) energy of the molecule. The molecule starts to rotate, vibrate and move parallel to the surface due to the corrugation and anisotropy of the PES. This dynamical trapping process is illustrated in Fig. 8. In this so-called dynamical precursor state [76, 77], the molecule does not have sufficient kinetic energy perpendicular to the surface to scatter back in the gas phase. It bounces back and forth with respect to the substrate, and with every bounce it dissipates further energy to the substrate until after about $2\,ps$ it has accommodated at

the surface. The dynamical trapping of O_2 on Pt(111) depends relatively weakly on the initial kinetic energy which causes the leveling off of the trapping probability at higher kinetic energies.

It is important to realize that the dependence of the sticking probability of O_2 on Pt(111) as just discussed can only be understood using dynamical simulations and concepts. Static information alone is not sufficient to derive these results.

VI. ADSORPTION DYNAMICS ON PRECOVERED SURFACES

In sect. IV we have already seen, that precovering a surface can significantly influence the adsorption and reaction dynamics on a surface. However, during the course of a reaction in heterogeneous catalysis the reactants themselves remain for a certain period of time on the surface. and block adsorption sites. Furthermore, their presence can also influence the electronic structure of the substrate and thus the reactivity of the catalyst [78]. Last but not least, the recoil of the substrate and thus the dissipation of the energy of impinging molecules will be modified.

To model coverage effects in the adsorption dynamics corresponds to a high-dimensional problem in which several inequivalent atoms have to be realistically described. An analytical or numerical interpolation of such a high-dimensional interaction potential is rather cumbersome but can be managed [24]. Fortunately, due to the increase in computer power and the development of efficient electronic structure codes it is now possible to perform *ab initio* molecular dynamics (AIMD) simulations of complex systems in which the forces necessary to integrate the equations of motion are determined "on the fly" by first-principles calculations. While some years ago AIMD studies were restricted to a small number of trajectories [79, 80], now a statistically meaningful number of AIMD trajectories can be determined, as has already been demonstrated [9, 24, 25, 81, 82].

The interest in the adsorption at precovered surface was fueled by a recent STM study [83, 84] which showed that cold H_2 molecules impinging on an almost completely hydrogen-covered Pd(111) surface do not adsorb dissociatively in a hydrogen dimer vacancy. Rather, aggregates of three or more vacancies are required to dissociate hydrogen. A subsequent DFT study [85] demonstrated that the presence of the hydrogen overlayer has a poisoning effect; it leads to the formation of energetic barriers making the dissociative adsorption on hydrogen-precovered Pd(111) to an activated process, but the dissociative adsorption of H_2 in a hydrogen dimer vacancy is still exothermic.

These findings were confirmed in a AIMD study [9]: at low initial kinetic energies of $0.02\,eV$, as used in the experiments [83, 84], H_2 molecules are not able to overcome the dissociation barrier above a dimer vacancy on
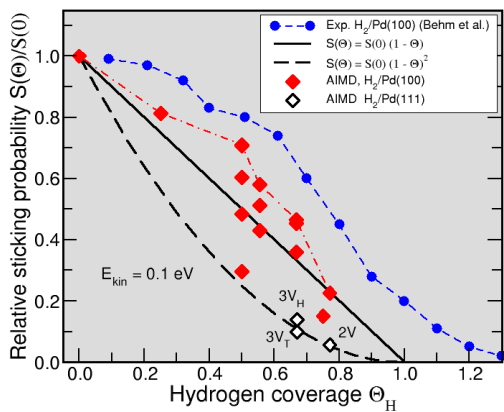
FIG. 9: Relative dissociative adsorption probability of hydrogen on hydrogen-covered Pd(100) determined through AIMD simulations as a function of hydrogen coverage θ_H involving different arrangements of the hydrogen. The initial kinetic energy is 0.1 eV. 2V, $3V_H$ and $3V_T$ denote the dimer vacancy and the trimer vacancy centered around a Pd hollow and a Pd top site on Pd(111), respectively. The experimental results [86] were obtained for a temperature of 170 K (after [82]).

H-covered Pd(111) surface within a (3×3) geometry corresponding to a surface coverage of $\Theta_H = 7/9 \approx 0.78$. At higher kinetic energies, however, H_2 molecules can penetrate the dimer vacancies on hydrogen-covered Pd(111) and adsorb dissociatively.

This is shown in Fig. 9 where the sticking probabilities on both Pd(111) and Pd(100) are plotted as a function of the hydrogen coverage for different arrangements of the pre-adsorbed hydrogen normalized to the value at the corresponding clean Pd surfaces for an kinetic energy of 0.1 eV. The results were obtained by averaging over at least 200 trajectories for each coverage. Hydrogen dimer and trimer vacancies were modeled within a (3×3) surface periodicity corresponding to hydrogen coverages of 7/9 and 2/3, respectively. As far as the dimer vacancy on Pd(111) is concerned (denoted by 2V in Fig. 9), a small, but non-vanishing relative adsorption probability of 0.05 is obtained. At the trimer vacancies on Pd(111) centered either around a hollow site ($3V_H$) or a Pd top site ($3V_T$), the adsorption probability is more than twice as large as on the dimer vacancy (2V). Since the area of the trimer vacancy is only 50% larger than the one of the dimer vacancy, this indicates that it is not only the area of the vacancies that determines the adsorption probability but also indirect poisoning and dynamical effects.

These dynamical effects in the adsorption at precovered surfaces have been studied in greater detail at the more open Pd(100) surface. As a reference, two curves corresponding to $S(\Theta_H) = S(0)(1 - \Theta_H)$ and $S(\Theta_H) = S(0)(1 - \Theta_H)^2$ are included in Fig. 9 which would correspond to the sticking probability if it was determined by pure site-blocking requiring one or two empty sites, respectively. For Pd(111), the AIMD results are close

to those predicted for site-blocking requiring one empty site. However, for the more open and reactive Pd(100) surface where the adsorption into a dimer vacancy is non-activated, the sticking probability is significantly larger than predicted from a simple site-blocking picture, in particular for $\Theta_H = 0.5$. This is somewhat surprising since the hydrogen coverage leads to a small poisoning effect which should reduce the sticking probability. Yet, because there is no mass mismatch between the impinging hydrogen molecules and the adsorbed hydrogen atoms, there should be a larger energy transfer to the substrate. In order to check the dynamical role of the surface atoms, additional AIMD runs with fixed substrate atoms were performed [9]. This showed that it is indeed the energy transfer from the impinging H_2 molecule to the substrate that leads to this enhanced sticking probability compared to pure site blocking. Still, also the rearrangement of the substrate atoms when the incoming H_2 molecules strike the strongly corrugated surface contributes to the high sticking probability. In Fig. 9, also experimental results [86] are included. These are obtained for lower kinetic energies than the one used in the AIMD simulations, hence the experimental and theoretical results are not directly comparable. It should also be noted that the theoretical results for each coverage should in principle be averaged over a statistical ensemble of different surface structures with the same coverage. Still it is gratifying that the calculated maximum sticking probabilities trail the experimental results.

The AIMD simulations do not only yield statistically reliable sticking probabilities, they also allow for valuable microscopic insights into the dissociative adsorption dynamics. Many impinging molecules either directly dissociate on the surface or scatter back into the gas phase. However, in some cases it takes some while before the adsorbing H_2 molecules end up in the energetically most favorable hollow sites on hydrogen-covered Pd. This is illustrated in Fig. 10 where snapshots of an adsorption trajectory at a H(3×3)/Pd(100) surface with a hydrogen coverage of 5/9 are shown. The H_2 molecule first hits the Pd surface close to a Pd top site where it becomes dynamically trapped [57, 76, 77] above the Pt top site (see Fig. 10a): the molecule does not directly find the pathway towards dissociation, but starts rotating, vibrating and moving laterally, and due the conversion of the initial kinetic energy into internal and lateral degrees of freedom, the H_2 molecule can not escape back into the gas phase. This molecular precursor state above the top sites is stabilized due to the poisoning effects of the pre-adsorbed hydrogen atoms, very similar to the one already identified at the hydrogen-covered stepped Pd(210) surface [87, 88]. It corresponds to a PdH$_2$ complex which is known in the gas phase [89] with the H_2 molecule moving relatively freely around the ontop position. This state has not been identified experimentally yet, however, it should be detectable at low surface temperatures by, e.g., isotope exchange experiments since it is bound by 0.1 eV.
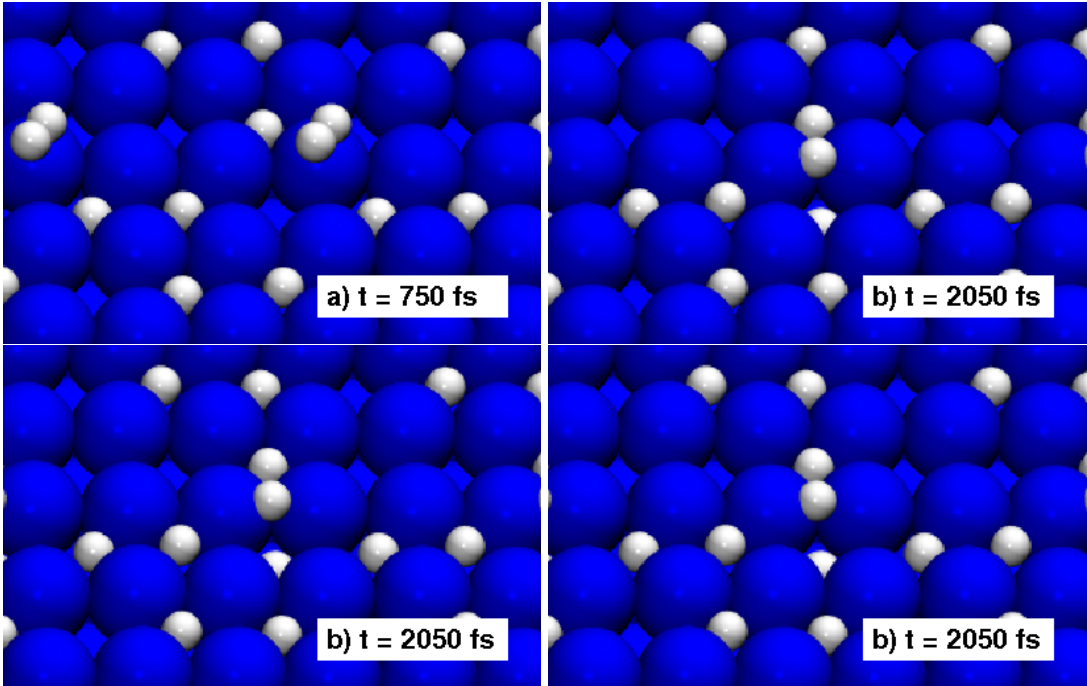
FIG. 10: Snapshots of a trajectory calculated in *ab initio* molecular dynamics simulations [9] within a (3×3) surface periodicity illustrating details of the adsorption dynamics at a hydrogen-covered Pd(100) surface. a) Molecular precursor, b) dissociation into hydrogen atoms in the four-fold hollow and the bridge site, c) exchange diffusion of the bridge-bonded hydrogen atom, d) final adsorption in four-fold hollow site by a exchange mechanism.

After about $2\,\mathrm{ps}$, one of the two hydrogen atoms of the impinging H_2 molecule enters the energetically most favorable adsorption site, the four-fold hollow site (Fig. 10b). The associated energy gain of about $0.5\,\mathrm{eV}$ is transfered to the hydrogen overlayer which results in large vibrational amplitudes of the hydrogen atoms. This is visible as the large displacements of some of the hydrogen atoms from their equilibrium sites. However, the other hydrogen atom does not directly find another four-fold hollow sites but becomes trapped at a bridge-bonded site.

The additional bridge-site hydrogen atom is not immobile but can actually move along the surface in an exchange mechanism [90]: after $3.4\,\mathrm{ps}$ it replaces one of the adsorbed hydrogen atoms at the four-fold hollow sites which is then pushed up to an adjacent bridge site (Fig. 10c). In fact, several of these exchange processes occur until finally after $5\,\mathrm{ps}$ the bridge-bonded hydrogen atoms pushes an adsorbed hydrogen atom to another empty four-fold hollow site (Fig. 10d). Still it takes some time before the hydrogen atoms dissipate the energy gained upon entering the adsorption wells. This is reflected in some atomic jumps between adjacent atomic hydrogen adsorption sites (not shown in Fig. 10) and will be discussed in the next section.

It is important to realize that some of the processes just described are not at all obvious. Thus by following the time evolution of the adsorption dynamics obtained by AIMD simulations, interesting and unexpected insights into the reaction dynamics at surfaces can be gained.

VII. RELAXATION DYNAMICS OF DISSOCIATED H_2 MOLECULES

In the last section we have focused on the dissociation of H_2 on hydrogen-covered Pd surfaces. We followed the H_2 dissociation dynamics on Pd, but we did not really consider the fate of the hydrogen atoms after the dissociation. However, directly after the dissociation the atoms gain a significant amount of energy when they enter the atomic adsorption wells, which amounts to about $1\,\mathrm{eV}$ for the two H atoms together on Pd surfaces. Since it takes some time before this excess kinetic energy is dissipated to the substrate, the energy gain leads to the formation of "hot" atoms, i.e., atoms with energies much larger than thermal energies. These atoms can use their kinetic energy in order to propagate along the surface. The mean free path of these hot atoms is for example relevant for catalytic reactions on surfaces since it determines whether adjacent reactants can react directly after the dissociative adsorption with another species or whether some diffusive motion is required before any further reaction can occur.

There are some theoretical studies that modeled the motion of single atoms with initial velocities considered to be typical for dissociation fragments directly after the bond-breaking process [91, 92] in order to address the re-
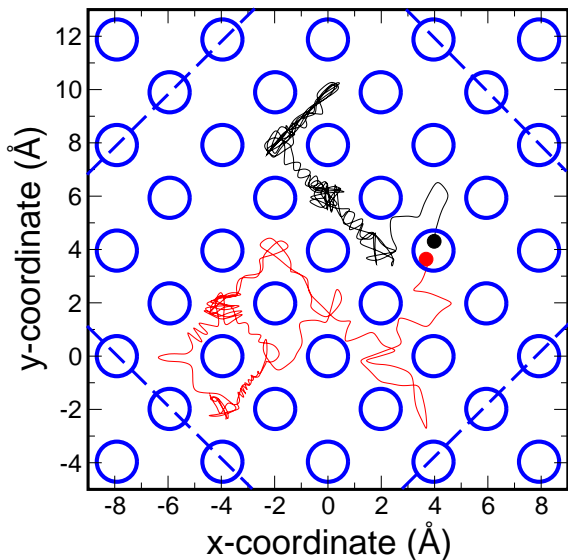
FIG. 11: Illustration of a trajectory of the hydrogen atoms after dissociation on clean Pd(100) within a (6×6) surface unit cell. The initial kinetic energy was $0.2\,\mathrm{eV}$. The total run time was $2\,\mathrm{ps}$. The surface unit cell of the simulations is indicated by the dashed blue line.
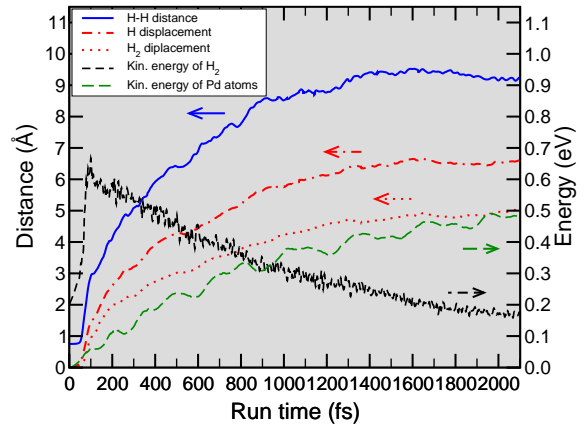

FIG. 12: Calculated hot atom dynamics after H_2 dissociation on clean Pd(100) within a (6×6) surface unit cell. H-H distance, the displacement of the single H atoms and the H_2 center of mass from their initial lateral position, the kinetic energy of the H_2 molecules and of the Pd substrate as a function of the run time averaged over 100 AIMD trajectories with an initial H_2 kinetic energy of $200\,\mathrm{meV}$.

laxation of hot atoms after dissociation. However, in such simulations the interaction of the two fragments after the dissociation is not taken into account. This approximation has been avoided in AIMD simulations of the dissociation of H_2 on clean Pd(100) based on periodic DFT calculations [81]. In order to minimize the interaction of the hot hydrogen atoms with their periodic images, a large (6×6) surface unit cell was chosen.

Figure 11 displays one specific AIMD trajectory that was run for $2\,\mathrm{ps}$. The trajectory shows that the single hydrogen atoms visit several surface sites before they come to rest. In this particular trajectory, the hydrogen atoms approach each other again after an initial increase in the interatomic distance. At a certain time, they are moving towards adjacent adsorption sites before they separate again. This shows that the mutual interaction can be important for the hot atom movement.

The displacement of the hydrogen atom and their energy redistribution as a function of time averaged over 100 AIMD trajectories is plotted in Fig. 12. The initial kinetic energy was chosen to be 0.2 eV in order to avoid molecular trapping events. Running trajectories with other initial kinetic energies shows that the hot atom movement is only weakly dependent on the initial kinetic energy since most of the kinetic energy is provided by the energy gain upon dissociative adsorption.

In detail, the mean H-H distance, the mean displacement of the single H atoms and the H_2 center of mass and the total kinetic energy of the hydrogen and the palladium atoms are plotted in Fig. 12. Directly after hitting the surface, the H_2 molecules dissociate and gain on the average about $700\,\mathrm{meV}$ when the hydrogen atoms enter adjacent atomic adsorption wells. Because of this high kinetic energy, the hydrogen atoms make further jumps and increase their separation. At the same time, they constantly lose kinetic energy that is transfered to the substrate.

After about $1\,\mathrm{ps}$ the hydrogen atoms have lost half of their kinetic energy, their joined mean kinetic energy is about $0.3\,\mathrm{eV}$. The mean separation of the two hydrogen atoms then levels off at a value of about $9\,\mathrm{Å}$ which corresponds to about three Pd lattice units. However, there is a large variance in the separation, single trajectories show a maximum H-H distance of more than $20\,\mathrm{Å}$. The single hydrogen atoms have moved two lattice sites on the average but also the H_2 center of mass is displaced by about $5\,\mathrm{Å}$ from its initial lateral position. After $2\,\mathrm{ps}$, the atoms have less than $0.2\,\mathrm{eV}$ kinetic energy left, and their mean displacement does not change any more. It is interesting to note that this kinetic energy is still larger than the diffusion barrier of hydrogen atoms on Pd(100) which is about $30\,\mathrm{meV}$, but the irregular motion of the hydrogen atoms does not lead to a further net displacement.

Further AIMD trajectories have been determined for a fixed substrate with and without rescaling of the velocities. In addition, AIMD runs were carried out in which the two single hydrogen atoms after the initial dissociation moved separately of each other [81]. It turned out that whereas any single trajectory depends sensitively on the specific conditions, on the average it is just the energy dissipation that determines the final mean distance of the two dissociation products; the mutual interaction of the two fragments plays a minor role, at least for H_2 dissociation on Pd(100).

Hydrogen is the lightest element and thus should show the smallest energy transfer to substrate atoms because

of the mass mismatch. Hence the results for the hot atom motion of hydrogen should represent an upper limit for other heavier atoms such as oxygen or nitrogen which dissipate their energy more quickly to metal substrates. Thus the hot atom motion should lead to mean displacements of at most three lattice sites. Wider separations [93] should be due to other processes, such as the so-called cannon-ball mechanism [94] where one atom in dissociative adsorption is emitted again and re-impinges on the surface at a laterally distant site.

VIII. ELECTRONICALLY NONADIABATIC REACTION DYNAMICS

So far we have always assumed that the Born-Oppenheimer approximation is valid for the description of the reaction dynamics on surfaces. As long as there is a satisfactory agreement between electronically adiabatic simulations and experiment, there is no need to invoke electronic excitations in the dynamics [42]. Still there are dynamical processes where electronic excitations play an important role. One has to distinguish between two kinds of electronic excitations in the reaction dynamics at surfaces, delocalized excited states of the surface and localized excitations at the reactant or the adsorbate-surface bond. The first type corresponds to electron-hole pair excitations which exhibit a continuous spectrum, in particular at metal surfaces, and which can often been described using a friction formalism. Using a *molecular dynamics with electronic friction* approach [95] based on Hartree-Fock cluster calculations, it was shown that the excitations of electron hole pairs upon the adsorption of CO on Cu(100) has only a minor influence on the sticking probability [96]. This is illustrated in Fig. 13: taking into account energy dissipation to electron-hole pairs increases the sticking probability only slightly since the main channel for energy transfer is the excitation of substrate vibrations.

On the other hand, using thin polycrystalline metal and semiconductor films deposited on n-type Si(111) as a Schottky diode device, the so-called chemicurrent due to nonadiabatically generated electron-hole pairs upon both atomic and molecular chemisorption can be measured [97–99]. For the NO adsorption on Ag, it has been estimated that one quarter of the adsorption energy of about 1 eV is dissipated to electron-hole pairs.

The generation of the chemicurrent upon adsorption has been addressed in several theoretical studies [100–104]. Based upon time-dependent density-functional theory (TDDFT), the excitation of electron-hole pairs in the atomic hydrogen adsorption on Al(111) was studied from first-principles [103, 104]. The dynamics of the nuclei were treated in the mean-field approximation whereas the time evolution of the electron system was determined by integrating the time-dependent Kohn–Sham equations. However, because of the light mass of the electrons, a rather short time step had to be chosen which was of the
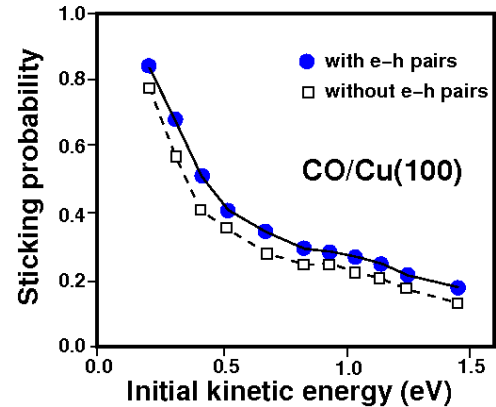

FIG. 13: Calculated sticking probability for CO/Cu(100) under normal incidence calculated without and with the consideration of electronic friction illustrating the minor role of e–h pairs in the molecular adsorption (after [96]).

order of $0.002 - 0.003$ fs [103, 104] which is about three orders of magnitude smaller than the time step required for electronically adiabatic molecular dynamics simulations. Therefore only very few selected trajectories could be calculated.

These simulations showed that the excitation of electron-hole pairs depends sensitively on the impact point of the hydrogen atom. If the hydrogen atom impinges at the Al(111) fcc hollow site, it penetrates into the Al crystal and couples strongly to the substrate electrons so that the energy loss to electron-hole pairs and phonons becomes comparable. At the ontop site, on the other hand, the energy dissipated to electron-hole pairs is much smaller, below 0.1 eV, whereas there is still a significant energy transfer to the phonons [103].

Note that there are also nonadiabatic effects as far as the spin of the hydrogen atom is concerned. Far away from the surface, the H atom is spin-polarized since there is only one electron with a specific spin, while it becomes spin-unpolarized upon adsorption on Al(111). The TDDFT-AIMD simulations showed [104], in agreement with simulations based on the Newns-Andersen model [102], that the hydrogen atom approaching the surface does not follow the adiabatic spin ground state because of the weak coupling between the spin states. These nonadiabatic spin dynamics lead to additional electronic dissipation.

Spin effects are also believed to be crucial in the system O_2/Al(111). The sticking of O_2 on Al(111) has represented a puzzle for a long time: On the one hand, molecular beam experiments yield a vanishing sticking probability at low kinetic energies and thus suggest that the adsorption is hindered by a small adsorption barrier [93, 105]. On the other hand, adiabatic electronic structure calculations using DFT yield a potential energy surface with large purely attractive portions [107–109] so that the dissociation probability for all kinetic energies should be close to one. This is demonstrated in Fig. 14
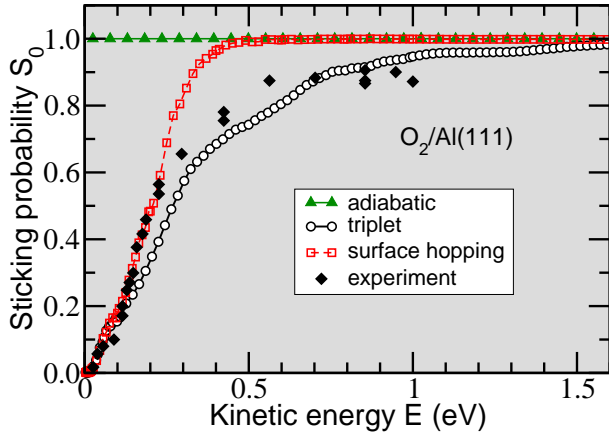
FIG. 14: Sticking probability of $O_2/Al(111)$ as a function of the kinetic energy for normal incidence computed by MD simulations on the adiabatic ($\triangle$) and triplet ($\circ$) PES, as well as by a surface hopping (SH) method including both the triplet and the singlet PES ($\square$). The experimental data ($\blacklozenge$) are taken from Ref. [105] (after [106]).
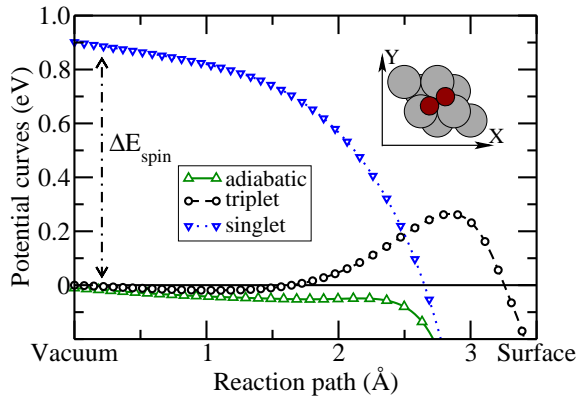

FIG. 15: Minimum energy pathway in the triplet state and corresponding adiabatic and singlet potentials for dissociation over the fcc site, with the molecular axis aligned parallel to the surface, as derived from constrained DFT calculations [110]. ΔE_{spin} indicates the singlet-triplet splitting in the gas phase. The inset illustrates the molecular configuration.

where the experimentally measured sticking probability is contrasted with the MD results based on the adiabatic DFT-PES [110].

To resolve this puzzle, it was proposed that spin selection rules play an important role in understanding the dissociation dynamics of $O_2/Al(111)$ [110–112]. Upon adsorption, oxygen changes its spin state from the gas-phase $^3\Sigma_g^-$ triplet state to the singlet state. Because of the low density of states of aluminum at the Fermi level, the probability for the triplet-to-singlet transition is rather small. Hence the O_2 molecules do not follow the adiabatic potential energy curve but rather stay in the triplet state which becomes repulsive close to the surface.

The shape of the spin-dependent potential energy curves of $O_2/Al(111)$ is illustrated in Fig. 15. The

triplet curve is obtained within a constrained DFT formalism [110–112] in which an auxiliary magnetic field was introduced in order to keep O_2 in its triplet state. The first excited state of the system is modeled by an adiabatic spin-unpolarized DFT calculation, leading to an approximate description of the singlet state. In the triplet state, O_2 adsorption is no longer non-activated but hindered by a small barrier whereas for the singlet state there are purely attractive adsorption paths.

Classical MD simulations were performed on the triplet PES interpolated by a neural network [20] with the Al substrate atoms kept fixed. The resulting sticking probability is also included in Fig. 14 denoted as triplet. Due to the presence of a minimum adsorption barrier, the triplet results are in good agreement with the experiment.

Still, in these simulations triplet-singlet transitions were completely neglected. Since the adiabatic, triplet and singlet PESs are known, the coupling matrix elements between singlet and triplet states can be derived by inverting the diagonalization of the diabatic Hamiltonian. Using these coupling elements, molecular dynamics simulations including electronic transitions were performed using the Fewest Switches algorithm [113–115]. In this surface hopping method, the nuclear degrees of freedom are integrated classically on one potential energy surface at each time step. Simultaneously, the density matrix including all electronic states is calculated by integrating the time–dependent Schrödinger equation along this trajectory. Transitions from one PES to another are introduced in such a way that for a large number of trajectories the occupation probabilities given by the density matrix are achieved within the smallest number of switches possible [113, 115].

Including triplet-singlet transitions in the adsorption dynamics of O_2 on Al(111) leads to an increase in the sticking probability at intermediate energies, as the surface hopping results included in Fig. 14 demonstrate [106, 116]. Molecules with low kinetic energies are scattered at the repulsive triplet potential before they can reach the region where the triplet-singlet transitions occur with a significant probability. However, O_2 molecules with intermediate energies can reach this region, where the transition from the activated triplet PES to the attractive singlet PES facilitate the dissociative adsorption and thus increase the sticking probability.

Still it should be noted that the inclusion of triplet-singlet transitions changes the sticking probability with respect to the pure triplet results only quantitatively, not qualitatively. Furthermore, the experimental sticking curve could also be reproduced in a purely electronically adiabatic framework on a slightly changed PES. It might well be that an improved description of exchange and correlation effects in the adiabatic DFT calculations would lead to the presence of an activation barrier [117, 118]. Hence the sticking probability of triplet O_2 does not allow an unequivocal assessment of the role of spin transitions in the O_2-Al interaction dynamics.

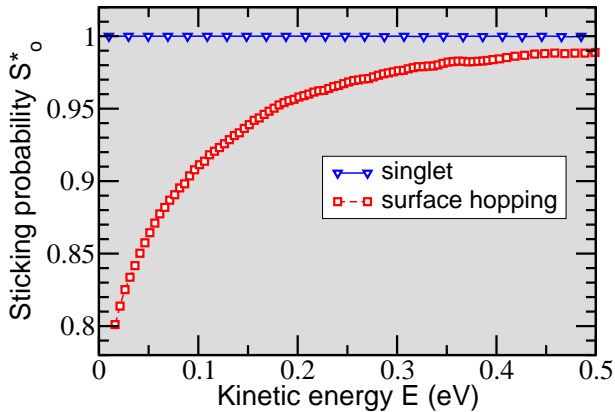It was therefore suggested to consider the adsorption of

FIG. 16: Sticking probability for singlet oxygen molecules ($^1\Delta_g$) impinging on Al(111) as computed by molecular dynamics simulations on the singlet PES ($\triangledown$) and by the fewest switches surface hopping algorithm ($\square$) based on first-principles calculations (after [106]).

singlet O_2 molecules on Al(111). This is experimentally well feasible, as was just demonstrated for the adsorption of O_2 on small Al_n clusters [119]. If all impinging O_2 molecules stayed in the singlet state, the sticking probability would be unity, as shown in Fig. 16 where the calculated sticking probability for O_2 molecules on the singlet PES is plotted. Allowing spin transitions, however, leads to a significant reduction of the singlet sticking probability. This is due to the fact that some of the impinging singlet molecules that suffer a spin transition near the crossing seam of the singlet and triplet PES are back-scattered on the triplet PES which indeed exhibits some barriers larger than 1 eV. Furthermore, upon the singlet-triplet transition, the possible energy gain is not all transfered into the propagation along the reaction path but also into other molecular degrees of freedom which also reduces the sticking probability. These effects lead to a measurable reflection probability for singlet molecules approaching Al(111) with a low kinetic energy.

Even if the experimental molecular beam does not completely consist of singlets, it would still be possible to discriminate the non-adiabatically reflected molecules. All reflected singlet molecules leave the surface in the triplet state. However, this also means that the difference between the O_2 singlet and triplet energy $\Delta E_{\rm spin}$ (indicated in Fig. 15) becomes released during the scattering event. Due to the redistribution of this excess energy, the reflected molecules become translationally, vibrationally and rotationally hot, i.e., upon reflection they gain a significant amount of energy in all molecular degrees of freedom. Their energy distribution thus provides an unequivocal signature for the non-adiabatic spin

transition.

IX. CONCLUSIONS

Due to the improvement of the computer power and the development of efficient algorithms it is now possible to reliably simulate the dynamics of reactions at surfaces from first-principles, i.e., without invoking any empirical parameter. Thus detailed insights into reaction mechanisms in heterogeneous catalysis can be gained. However, the simulations are not only limited to explanatory purposes but also gain a predictive power, as demonstrated for the case of spin effects in the interaction of singlet O_2 with Al(111) in this overview.

Still, most of the reactants addressed in the presented dynamical simulations are still rather simple, as mainly diatomic molecules were considered. In particular in ab initio molecular dynamics simulations it is in principle no problem to treat more complex molecules. Hence we will certainly see dynamical studies including more complex catalytically relevant molecules such a methanol in the future.

On the other hand, dynamical simulations are typically restricted to a rather short time scale only up to pico- or at most nanoseconds. This means that they can often only treat specific steps of a catalytic reaction. In particular rare processes hindered by large activation barriers are usually out of reach for dynamical simulation. Nevertheless, within a multi-scale approach, either involving horizontal coupling (hybrid methods) or vertical coupling (parameter inheritance), as described elsewhere in this volume, dynamical simulations are an indispensable tool for a complete understanding of catalytic reactions at surfaces.

[1] Kroes, G.-J. *Science* **2008**, *321*, 794.

[2] Groß, A. *Theoretical surface science – A microscopic*

perspective; Springer: Berlin, 2nd ed., 2008.

[3] Nørskov, J. K.; Abild-Pedersen, F.; Studt, F.; Bligaard, T. *Proc. Natl. Acad. Sci.* **2011**, *108*, 937–943.

[4] Hänggi, P.; Talkner, P.; Borkovec, M. *Rev. Mod. Phys.* **1990**, *62*, 251.

[5] Cucchetti, A.; Ying, S. C. *Phys. Rev. B* **1996**, *54*, 3300–3310.

[6] Fichthorn, K. A.; Weinberg, W. H. *J. Chem. Phys.* **1991**, *95*, 1090.

[7] Sendner, C.; Sakong, S.; Groß, A. *Surf. Sci.* **2006**, *600*, 3258.

[8] Groß, A. In *The Chemical Physics of Solid Surfaces*; Woodruff, D. P., Ed., Vol. 11; Elsevier: Amsterdam, 2003; chapter 1.

[9] Groß, A.; Dianat, A. *Phys. Rev. Lett.* **2007**, *98*, 206107.

[10] Born, M.; Oppenheimer, J. R. *Ann. Phys.* **1927**, *84*, 457.

[11] Groß, A.; Wei, C. M.; Scheffler, M. *Surf. Sci.* **1998**, *416*, L1095.

[12] Wiesenekker, G.; Kroes, G.-J.; Baerends, E. J. *J. Chem. Phys.* **1996**, *104*, 7344.

[13] Groß, A.; Scheffler, M. *Phys. Rev. B* **1998**, *57*, 2493.

[14] Wei, C. M.; Groß, A.; Scheffler, M. *Phys. Rev. B* **1998**, *57*, 15572.

[15] Hammer, B.; Scheffler, M.; Jacobsen, K.; Nørskov, J. *Phys. Rev. Lett.* **1994**, *73*, 1400.

[16] Blank, T. B.; Brown, S. D. Calhoun, A. W.; Doren, D. J. *J. Chem. Phys.* **1995**, *103*, 4129.

[17] No, K. T.; Chang, B. H.; Kim, S. Y.; Jhon, M. S.; Scheraga, H. A. *Chem. Phys. Lett.* **1997**, *271*, 152.

[18] Lorenz, S.; Groß, A.; Scheffler, M. *Chem. Phys. Lett.* **2004**, *395*, 210.

[19] Lorenz, S.; Scheffler, M.; Groß, A. *Phys. Rev. B* **2006**, *73*, 115431.

[20] Behler, J.; Lorenz, S.; Reuter, K. *J. Chem. Phys.* **2007**, *127*, 014705.

[21] Crespos, C.; Collins, M. A.; Pijper, E.; Kroes, G.-J. *Chem. Phys. Lett.* **2003**, *376*, 566.

[22] Busnengo, H. F.; Salin, A.; Dong, W. *J. Chem. Phys.* **2000**, *112*, 7641.

[23] Kresse, G. *Phys. Rev. B* **2000**, *62*, 8295.

[24] Lozano, A.; Groß, A.; Busnengo, H. F. *Phys. Rev. B* **2010**, *81*, 121402(R).

[25] Lozano, A.; Groß, A.; Busnengo, H. F. *Phys. Chem. Chem. Phys.* **2009**, *11*, 5814.

[26] McCormack, D. A.; Olsen, R. A.; Baerends, E. J. *J. Chem. Phys.* **2005**, *122*, 194708.

[27] Salin, A. *J. Chem. Phys.* **2006**, *124*, 104704.

[28] Mehl, M. J.; Papaconstantopoulos, D. A. *Phys. Rev. B* **1996**, *54*, 4519.

[29] Goringe, C. M.; Bowler, D. R.; Hernández, E. *Rep. Prog. Phys.* **1997**, *60*, 1447.

[30] Groß, A.; Scheffler, M.; Mehl, M. J.; Papaconstantopoulos, D. A. *Phys. Rev. Lett.* **1999**, *82*, 1209.

[31] Slater, J. C.; Koster, G. F. *Phys. Rev.* **1954**, *94*, 1498.

[32] Groß, A.; Eichler, A.; Hafner, J.; Mehl, M. J.; Papaconstantopoulos, D. A. *Surf. Sci.* **2003**, *539*, L542.

[33] Groß, A.; Eichler, A.; Hafner, J.; Mehl, M. J.; Papaconstantopoulos, D. A. *J. Chem. Phys.* **2006**, *124*, 174713.

[34] Newton, R. *Scattering Theory of Waves and Particles;* Springer: New York, second ed., 1982.

[35] Fleck, J. A.; Morris, J. R.; Feit, M. D. *Appl. Phys.* **1976**, *10*, 129.

[36] Tal-Ezer, H.; Kosloff, R. *J. Chem. Phys.* **1984**, *81*, 3967.

[37] Kroes, G.-J. *Prog. Surf. Sci.* **1999**, *60*, 1.

[38] Groß, A. *Surf. Sci. Rep.* **1998**, *32*, 291.

[39] Groß, A. *Theoretical surface science – A microscopic perspective;* Springer: Berlin, 2002.

[40] Groß, A.; Wilke, S.; Scheffler, M. *Phys. Rev. Lett.* **1995**, *75*, 2718.

[41] Kroes, G.-J.; Baerends, E. J.; Mowrey, R. C. *Phys. Rev. Lett.* **1997**, *78*, 3583.

[42] Nieto, P.; Pijper, E.; Barredo, D.; Laurent, G.; Olsen, R. A.; Baerends, E.-J.; Kroes, G.-J.; Farias, D. *Science* **2006**, *312*, 86.

[43] Diaz, C.; Pijper, E.; Olsen, R. A.; Busnengo, H. F.; Auerbach, D. J.; Kroes, G. J. *Science* **2009**, *326*(5954), 832–834.

[44] Groß, A.; Scheffler, M. *Phys. Rev. B* **2000**, *61*, 8425.

[45] Olsen, R. A.; McCormack, D. A.; Luppi, M.; Baerends, E. J. *J. Chem. Phys.* **2008**, *128*, 194715.

[46] Rendulic, K. D.; Anger, G.; Winkler, A. *Surf. Sci.* **1989**, *208*, 404.

[47] Karikorpi, M.; Holloway, S.; Henriksen, N.; Nørskov, J. K. *Surf. Sci.* **1987**, *179*, L41.

[48] Wilke, S.; Scheffler, M. *Phys. Rev. Lett.* **1996**, *76*, 3380.

[49] Wilke, S.; Scheffler, M. *Phys. Rev. B* **1996**, *53*, 4926.

[50] Rutkowski, M.; Wetzig, D.; Zacharias, H.; Groß, A. *Phys. Rev. B* **2002**, *66*, 115405.

[51] Wetzig, D.; Rutkowski, M.; Zacharias, H.; Groß, A. *Phys. Rev. B* **2001**, *63*, 205412.

[52] Kroes, G.-J.; Groß, A.; Baerends, E. J.; Scheffler, M.; McCormack, D. A. *Acc. Chem. Res.* **2002**, *35*, 193.

[53] Rutkowski, M.; Wetzig, D.; Zacharias, H. *Phys. Rev. Lett.* **2001**, *87*, 246101.

[54] Rettner, C. T.; Auerbach, D. J.; Michelsen, H. A. *Phys. Rev. Lett.* **1992**, *68*, 1164.

[55] Rettner, C. T.; Michelsen, H. A.; Auerbach, D. J. *J. Chem. Phys.* **1995**, *102*, 4625.

[56] Cohen, A. J.; Mori-Sánchez, P.; Yang, W. *Science* **2008**, *321*, 792.

[57] Groß, A.; Scheffler, M. *J. Vac. Sci. Technol. A* **1997**, *15*, 1624.

[58] Rettner, C. T.; Auerbach, D. J. *Chem. Phys. Lett.* **1996**, *253*, 236.

[59] Groß, A.; Scheffler, M. *Phys. Rev. Lett.* **1996**, *77*, 405.

[60] Grimmelmann, E. K.; Tully, J. C.; Cardillo, M. J. *J. Chem. Phys.* **1980**, *72*, 1039.

[61] Kuipers, E. W.; Tenner, M. G.; Spruit, M. E. M.; Kleyn, A. W. *Surf. Sci.* **1988**, *205*, 241.

[62] Rettner, C. T.; Mullins, C. B. *J. Chem. Phys.* **1991**, *94*, 1626.

[63] Luntz, A. C.; Grimblot, J.; Fowler, D. E. *Phys. Rev. B* **1989**, *39*, 12903.

[64] Wurth, W.; Stöhr, J.; Feulner, P.; Pan, X.; Bauchspiess, K. R.; Baba, Y.; Hudel, E.; Rocker, G.; Menzel, D. *Phys. Rev. Lett.* **1990**, *65*, 2426.

[65] Steininger, H.; Lehwald, S.; Ibach, H. *Surf. Sci.* **1982**, *123*, 1.

[66] Puglia, C.; Nilsson, A.; Hernnäs, B.; Karis, O.; Bennich, P.; Mårtensson, N. *Surf. Sci.* **1995**, *342*, 119.

[67] Wintterlin, J.; Schuster, R.; Ertl, G. *Phys. Rev. Lett.* **1996**, *77*, 123.

[68] Eichler, A.; Hafner, J. *Phys. Rev. Lett.* **1997**, *79*, 4481.

[69] Eichler, A.; Mittendorfer, F.; Hafner, J. *Phys. Rev. B* **2000**, *62*, 4744.

[70] Nolan, P. D.; Lutz, B. R.; Tanaka, P. L.; Davis, J. E.; Mullins, C. B. *Phys. Rev. Lett.* **1998**, *81*, 3179.

[71] Nolan, P. D.; Lutz, B. R.; Tanaka, P. L.; Davis, J. E.; Mullins, C. B. *J. Chem. Phys.* **1999**, *111*, 3696.

[72] Luntz, A. C.; Williams, M. D.; Bethune, D. S. *J. Chem. Phys.* **1988**, *89*, 4381.

[73] Verlet, L. *Phys. Rev.* **1967**, *159*, 98.

[74] Sendner, C.; Groß, A. *J. Chem. Phys.* **2007**, *127*, 014704.

[75] Groß, A.; Scheffler, M. *Phys. Rev. B* **1998**, *57*, 2493.

[76] Busnengo, H. F.; Dong, W.; Salin, A. *Chem. Phys. Lett.* **2000**, *320*, 328.

[77] Crespos, C.; Busnengo, H. F.; Dong, W.; Salin, A. *J. Chem. Phys.* **2001**, *114*, 10954.

[78] Hammer, B. *Phys. Rev. B* **2001**, *63*, 205423.

[79] Groß, A.; Bockstedte, M.; Scheffler, M. *Phys. Rev. Lett.* **1997**, *79*, 701.

[80] Ciacchi, L. C.; Payne, M. C. *Phys. Rev. Lett.* **2004**, *92*, 176104.

[81] Groß, A. *Phys. Rev. Lett.* **2009**, *103*, 246101.

[82] Groß, A. *ChemPhysChem* **2010**, *11*, 1374.

[83] Mitsui, T.; Rose, M. K.; Fomin, E.; Ogletree, D. F.; Salmeron, M. *Nature* **2003**, *422*, 705.

[84] Mitsui, T.; Rose, M. K.; Fomin, E.; Ogletree, D. F.; Salmeron, M. *Surf. Sci.* **2003**, *540*, 5.

[85] Lopez, N.; Lodziana, Z.; Illas, F.; Salmeron, M. *Phys. Rev. Lett.* **2004**, *93*, 146103.

[86] Behm, R. J.; Christmann, K.; Ertl, G. *Surf. Sci.* **1980**, *99*, 320.

[87] Schmidt, P. K.; Christmann, K.; Kresse, G.; Hafner, J.; Lischka, M.; Groß, A. *Phys. Rev. Lett.* **2001**, *87*, 096103.

[88] Lischka, M.; Groß, A. *Phys. Rev. B* **2002**, *65*, 075420.

[89] Dedieu, A. *Chem. Rev.* **2000**, *100*, 543.

[90] Feibelman, P. J. *Phys. Rev. Lett.* **1990**, *65*, 729.

[91] Engdahl, C.; Wahnström, G. *Surf. Sci.* **1994**, *312*, 429.

[92] Pineau, N.; Busnengo, H. F.; Rayez, J. C.; Salin, A. *J. Chem. Phys.* **2005**, *122*, 214705.

[93] Brune, H.; Wintterlin, J.; Behm, R. J.; Ertl, G. *Phys. Rev. Lett.* **1992**, *68*, 624.

[94] Diebold, U.; Hebenstreit, W.; Leonardelli, G.; Schmid, M.; Varga, P. *Phys. Rev. Lett.* **1998**, *81*, 405.

[95] Head-Gordon, M.; Tully, J. C. *J. Chem. Phys.* **1995**, *103*, 10137.

[96] Kindt, J. T.; Tully, J. C.; Head-Gordon, M.; Gomez, M. A. *J. Chem. Phys.* **1998**, *109*, 3629.

[97] Gergen, B.; Nienhaus, H.; Weinberg, W. H.; McFarland, E. W. *Science* **2001**, *294*, 2521.

[98] Gergen, B.; Weyers, S. J.; Nienhaus, H.; Weinberg, W. H.; McFarland, E. W. *Surf. Sci.* **2001**, *488*, 123.

[99] Nienhaus, H. *Surf. Sci. Rep.* **2002**, *45*, 1.

[100] Trail, J. R.; Graham, M. C.; Bird, D. M. *Comp. Phys. Comm.* **2001**, *137*, 163.

[101] Trail, J. R.; Graham, M. C.; Bird, D. M.; Persson, M.; Holloway, S. *Phys. Rev. Lett.* **2002**, *88*, 166802.

[102] Mizielinski, M. S.; Bird, D. M.; Persson, M.; Holloway, S. *J. Chem. Phys.* **2005**, *122*, 084710.

[103] Lindenblatt, M.; van Heys, J.; Pehlke, E. *Surf. Sci.* **2006**, *600*, 3624.

[104] Lindenblatt, M.; Pehlke, E. *Phys. Rev. Lett.* **2006**, *97*, 216101.

[105] Österlund, L.; Zorić, I.; Kasemo, B. *Phys. Rev. B* **1997**, *55*, 15452–15455.

[106] Carbogno, C.; Behler, J.; Groß, A.; Reuter, K. *Phys. Rev. Lett.* **2008**, *101*, 096104.

[107] Sasaki, T.; Ohno, T. *Surf. Sci.* **1999**, *433*, 172.

[108] Honkala, K.; Laasonen, K. *Phys. Rev. Lett.* **2000**, *84*, 705.

[109] Y. Yourdshahyan, Y.; Razaznejad, B.; Lundqvist, B. I. *Phys. Rev. B* **2002**, *65*, 075416.

[110] Behler, J.; Delley, B.; Lorenz, S.; Reuter, K.; Scheffler, M. *Phys. Rev. Lett.* **2005**, *94*, 036104.

[111] Behler, J.; Delley, B.; Reuter, K.; Scheffler, M. *Phys. Rev. B* **2007**, *75*, 115409.

[112] Behler, J.; Reuter, K.; Scheffler, M. *Phys. Rev. B* **2008**, *77*, 115421.

[113] Tully, J. C. *J. Chem. Phys.* **1990**, *93*, 1061.

[114] Bach, C.; Klüner, T.; Groß, A. *Appl. Phys. A* **2004**, *78*, 231.

[115] Carbogno, C.; Groß, A.; Rohlfing, M. *Appl. Phys. A* **2007**, *88*, 579.

[116] Carbogno, C.; Behler, J.; Reuter, K.; Groß, A. *Phys. Rev. B* **2010**, *81*, 035410.

[117] Mosch, C.; Koukounas, C.; Bacalis, N.; Metropoulos, A.; Groß, A.; Mavridis, A. *J. Phys. Chem. C* **2008**, *112*, 6924.

[118] Bacalis, N. C.; Metropoulos, A.; Groß, A. *J. Phys. Chem. A* **2010**, *114*, 11746–11750.

[119] Burgert, R.; Schnöckel, H.; Grubisic, A.; Li, X.; Bowen, S. T. S. K. H.; Ganteför, G. F.; Kiran, B.; Jena, P. *Science* **2008**, *319*, 438.